# RIS-Aided MIMO Downlink Transmission for Ultra-Dense LEO Satellite-Terrestrial Networks

Xin Zhang, *Student Member, IEEE,* Xiaohan Qin, *Student Member, IEEE,* Zitian Zhang, Lin X. Cai, *Senior Member, IEEE,* Haibo Zhou, *Senior Member, IEEE,* and Weihua Zhuang, *Fellow, IEEE*

***Abstract*—Ultra-dense Low earth orbit (LEO) satellite-terrestrial network (ULSN) has evolved as a new paradigm to provide ubiquitous and high-capacity communications in next generation wireless networks. However, the direct LEO satellite broadband connectivity faces significant challenges in urban environments due to the masking effect, which limits the reliability and availability of communication links in ULSNs. To address this, reconfigurable intelligent surface (RIS) is emerging as a promising solution in ULSNs. In this paper, we investigate RIS-aided downlink data transmission in urban environments of multi-users in ULSNs. We set up a mixed-integer programming (MIP) model for maximizing the sum rate of terrestrial users in ULSNs. To solve the complex MIP problem, we propose a two-phase joint optimization (TPJO) algorithm with a deep learning phase and an alternative optimization (AO) phase. In the deep learning phase, a deep neural network (DNN) algorithm is employed to obtain the optimal user association matrix based on the positions of terrestrial users and LEO satellites. Then in the AO phase, successive convex approximation (SCA) is utilized to transform the nonconvex subproblems of beamforming and RIS phase design into convex formulations and iteratively solve them. Simulation results demonstrate that the proposed algorithm outperforms other baseline algorithms.**

***Index Terms*—Ultra-dense LEO satellite-terrestrial network, multiple-input multi-output, convex optimization, reconfigurable intelligent surface, deep neural network.**

## I. Introduction

With the burgeoning development of ultra-dense low earth orbit (LEO) satellite constellations, such as Starlink and OneWeb, the integration of LEO satellites with terrestrial networks has heralded a new paradigm for future sixth-generation (6G) networks [1], [2]. Ultra-dense LEO satellite-terrestrial network (ULSN) is expected to play a critical role not only in providing ubiquitous coverage to remote areas, but also delivering massive and high-capacity access in dense urban scenarios [3], [4]. In recent years, SpaceX's 'direct to cell' has emerged as a revolutionary integration architecture in ULSNs, which offers cellular connectivity and allows mobile users to directly connect to LEO satellites. However, for urban mobile users, high-rise buildings pose a major obstacle, often blocking the line-of-sight (LOS) paths necessary for effective communication between LEO satellites and mobile users, leading to a masking effect that impacts the efficiency and reliability of satellite-terrestrial communications [5]. Studies conducted by the Third Generation Partnership Project (3GPP) highlight this issue, indicating that in urban environments, the probability of maintaining a LOS connection between LEO satellites and terrestrial users can plummet to as low as 24.6% [6]. Consequently, the coverage area of LEO satellites in urban scenarios is reduced, resulting in limited service availability in ULSNs for mobile users on the street, which highlights the need for innovative solutions to address this limitation.

To overcome the masking effect of non-LOS (NLOS) paths and enhance the data transmission of ULSNs in urban environments, a promising emerging approach is the utilization of reconfigurable intelligent surfaces (RIS) [7]. Specifically, RIS is an electromagnetic metasurface consisting of a multitude of reconfigurable elements, each capable of independently controlling the reflected phase shift [8]. The cooperation of each independent RIS element can amplify the incident signal, enable the enhancement of power in the desired direction [9], resulting in finely-tuned passive beamforming gain. By intelligently reflecting and redirecting the signals, RIS placed on the exteriors of high-rise buildings can establish LOS links, facilitate street-level communication and dramatically improve the coverage and connectivity of ULSNs [10]. The RIS emerges as a critical and innovative element in ULSNs, offering more efficient integration for LEO satellites with terrestrial networks and a reduction in power consumption and complexity, particularly when compared to terrestrial relays in traditional satellite-terrestrial networks [11]. However, the successful deployment of RIS in urban environments of ULSNs faces several challenges. In multi-user scenarios, improper phase design of RIS elements can potentially exacerbate interference among users and degrade network performance [12]. Meanwhile, considering the high mobility of LEO satellites and propagation delay of satellite-terrestrial links, there is a high demand for low time-complexity algorithms in ULSNs. Additionally, the integration of RIS with existing ULSN infrastructure poses technical challenges, including requirements of efficient user association mechanisms, effective power allocations for users, signal propagation loss of satellite-terrestrial links. Therefore,

This work was supported in part by the National Key R&D Program of China under Grant 2020YFB1806104 and the Natural Science Fund for Distinguished Young Scholars of Jiangsu Province under Grant BK20220067. (*Corresponding author: Haibo Zhou.*)

X. Zhang, X. Qin and H. Zhou are with the School of Electronic Science and Engineering, Nanjing University, Nanjing 210023, China. (E-mail: zanxin@smail.nju.edu.cn, xhderemail@smail.nju.edu.cn, haibozhou@nju.edu.cn).

Z. Zhang is with the School of Information and Electronic Engineering, Zhejiang Gongshang University, Hangzhou 310018, China. (E-mail: zitian.zhang@mail.zjgsu.edu.cn).

L. X. Cai is with the Department of Electrical and Computer Engineering, Illinois Institute of Technology, Chicago, IL 60616, USA. (E-mail: lincai@iit.edu).

W. Zhuang is with the Department of Electrical and Computer Engineering, University of Waterloo, Waterloo, Ontario N2L 3G1, Canada. (E-mail: wzhuang@uwaterloo.ca).

to address these challenges, the development of effective low complexity algorithms for joint user association, beamforming and RIS phase design is critically important in ULSNs.

To the best of our knowledge, the utilization of RIS for enhancing the sum rate of LEO satellite downlink communications in ULSNs has not been investigated. In this paper, we investigate RIS-aided multiple-input multi-output (MIMO) downlink data transmission in the urban environments of multi-users in ULSNs. We formulate a mixed-integer programming (MIP) problem which aims at maximizing the sum rate of terrestrial users, while satisfying the transmit power budgets at LEO satellites. Due to the coupling of integer and continuous variables and the intractable non-convexity of the established MIP problem, we decouple the original problem into two phases. Subsequently, deep neural network (DNN) and alternating optimization (AO) are proposed to obtain the optimal user association and iteratively solve beamforming vectors and RIS phase shifts, respectively. Main contributions of this work are summarized as follows:

- *RIS-aided LEO downlink data transmission* - We focus on RIS aided LEO satellite-terrestrial MIMO downlink communication system in urban environment for multi-user scenario. A MIP problem considering power constraint of LEO and rate constraint of terrestrial users is formulated to maximize sum rate of terrestrial users in ULSN.
- *Two-phase joint optimization (TPJO)* - We propose a TPJO algorithm to decouple the original MIP problem into two phases, including a deep learning phase of integer programming that optimizes the user association, and an AO phase of continuous programming which jointly optimizes the beamforming and RIS phase shift.
- *DNN-based user association with LEO satellites* - We use the DNN algorithm to solve the integer programming of user association between terrestrial users and LEO satellites. Further, we train a fully connected neural network (FCNN) model to generate the association matrix based on the positions of terrestrial users and LEO satellites.
- *AO-based joint beamforming and RIS reflecting design* - We decompose the continuous programming problem into two subproblems including the beamforming optimization and RIS reflecting design, and jointly solve them through the AO approach. For each iteration in AO, we use the successive convex approximation (SCA) method to approximate the subproblems into convex for beamforming and RIS reflecting design, respectively.

The rest of this paper is structured as follows. Section II provides an overview of relevant works in the literature. Section III presents the system model and the problem formulation. Sections IV discusses the proposed algorithms to solve the formulated MIP problem. Section V provides numerical results to evaluate the proposed solutions. Finally, we draw conclusions in Section VI.

## II. Related Work

RIS has recently surfaced as a notable technological advancement in academia for achieving energy-efficient and high-spectrum efficiency in satellite communication systems. In RIS-aided satellite communication systems, RIS is placed either on the satellites to assist inter-satellite communications [13], [14] or near the ground to enhance the satellite-terrestrial microwave communications [15]–[21]. For instance, Zheng *et al*. propose an optimal beamforming and phase shifting design using a semi-definite programming (SDR) algorithm, maximizing the effective channel gain in single satellite and single-user scenarios of RIS-aided satellite communication in satellite-terrestrial integrated networks (STINs) [15]. To achieve high band utilization and channel quality, Cho *et al*. present a design for a dual-band RIS tailored for satellite network communication, which facilitates dynamic beamforming and frequency selection on different bands [10]. In [16], Dong *et al*. investigate the RIS-based secure cooperative transmission for STINs. They propose an AO scheme to minimize eavesdropper interference while maintaining target signal-to-interference-plus-noise Ratio (SINR) levels of each satellite users. Additionally, Liu *et al*. investigate uplink data transmission in STINs with the aid of RIS based on non-orthogonal multiple access, where a two-layer alternating algorithm is proposed to enhance the ergodic sum rate [20].

As the demand for high data transmission capacities grows, MIMO technologies are being increasingly integrated into satellite communications. You *et al.* delve into the feasibility and efficacy of LEO satellite communications utilizing MIMO techniques [22]. Their research reveals that the application of large-scale MIMO substantially improves the capacity and overall performance of satellite networks, presenting a significant improvement over traditional LEO satellite communication systems. Meanwhile, RIS is usually be applied to multi-antenna systems [19], which serves to elevate the quality and efficiency of communication in satellite networks demonstrating the versatility and impact of RIS technology [23]. Deng *et al.*'s work stands out by synergizing holographic MIMO with RIS, designing a multi-LEO satellite communication system that leverages holographic MIMO for dynamic beamforming [19]. This integration with RIS optimizes channel characteristics, marking a significant advancement in enhancing transmission rates and network reliability. In wireless communications including RIS-aided communication systems and STINs, machine learning as well as convex optimization is an effective tool for user association, beamforming design [24]–[26]. Sui *et al.* explore channel and power allocation in STINs using a two-step approach, combining convex optimization and DNN methods [24]. To maximize the secrecy rate in RIS-aided unmanned aerial vehicle networks, Yang *et al.* propose secure transmission scheme based on deep Q-network [25]. Meanwhile, Bie *et al.* propose a two-step fractional linearization algorithm for user association to maximize the minimal SINR among cell-free users [26].

Existing studies on RIS-aided satellite communications mainly concentrate on single-user or single-satellite contexts. As ULSNs evolve, the significance of multi-user and multi-satellite scenarios becomes increasingly pronounced for future development of ULSNs. Meanwhile, the high mobility of LEO satellites poses significant challenges to algorithmic complexity, particularly within multi-user and multi-satellite

scenarios of ULSNs. Therefore, it is necessary to design low-complexity algorithms for multiple terrestrial user scenarios to jointly optimize user association, beamforming and RIS phase design. Drawing inspiration from the preceding analysis, we explore the RIS-aided downlink data transmission in the urban environments of multiple terrestrial users in ULSNs. Low-complexity algorithms are designed to reduce the interference between multiple terrestrial users and improve the sum rate of multi-users with in a ULSN.

## III. System Model

As depicted in Fig. 1, we consider a MIMO downlink communication system with the aid of RIS in a ULSN. There are $N_S$ LEO satellites represented by $\mathcal{S} = \{1, 2, \ldots, N_S\}$ providing services to a terrestrial region, where each LEO satellite is equipped with $M_S$ uniform planar array (UPA) antennas. The RIS is strategically deployed on the outside wall of a high-rise building to assist the communication process. On the terrestrial front, we consider an urban environment densely populated with $N_U$ single-antenna users represented by $\mathcal{U} = \{1, 2, \ldots, N_U\}$. Using the three-dimensional (3D) Cartesian coordinate, the arrays of the LEO satellites serving this area are situated on the x-y plane, while the elements of the RIS are located on the x-z plane.

In satellite communication systems, time is partitioned into small slots. Within each slot, the relative network topology and channel state information (CSI) are considered static. Similar to the existing research [17], we consider a small relative time period where the system is quasi-static. Moreover, perfect CSI is assumed for all channels, which is achieved through the centralized radio access network architecture. The signal transmission from LEO satellites to terrestrial users occurs via two distinct pathways:

1) NLOS direct link: This involves the signal being transmitted directly from the LEO satellite to the terrestrial users, which suffers from masking effect and is usually blocked by urban high-rise buildings.
2) LOS reflect link: The signal is reflected via the RIS redirecting the LEO satellite's signal towards the terrestrial user. This link effectively bypasses obstacles that may obstruct the direct line of sight, potentially enhancing signal strength and reliability by providing an alternative path for the signal to reach the terrestrial user.

### A. Channel Model

In communication channel modelling, we take into account both large-scale fading (LSF) representing the path loss and shadowing effects over the long distances, and small-scale fading reflecting the rapid fluctuations in signal strength caused by factors such as multipath propagation. The LSF is given by [20]

$$L\left(d, f_c; -\eta\right) = \left(\frac{c}{4\pi f_c}\right)^2 d^{-\eta}, \tag{1}$$

where $c$ denotes the light speed, $d$ is the link distance, $f_c$ the carrier frequency, and $\eta$ the path loss coefficient.

We adopt the Rayleigh fading model for the NLOS direct link between LEO satellite and terrestrial user. The direct

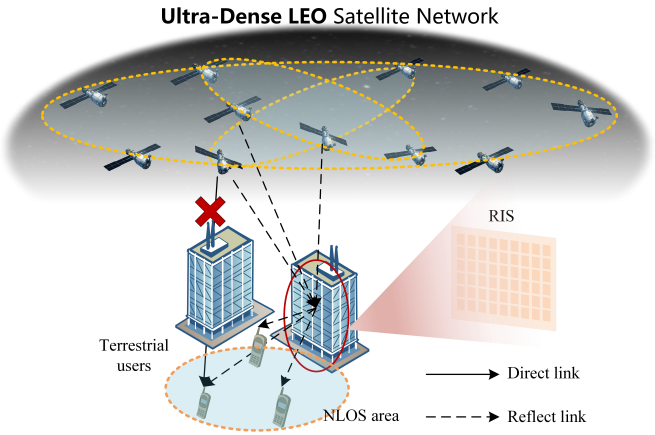


Fig. 1. RIS-aided LEO satellite-terrestrial downlink communications in urban environment.

channel gain $\mathbf{g}_{m,k} \in \mathbb{C}^{M_S \times 1}$ between the $m$-th LEO satellite and the $k$-th terrestrial user is given by

$$\mathbf{g}_{m,k} = \sqrt{G_S G_U L_{m,k}}\tilde{\mathbf{g}}_{m,k}, \tag{2}$$

where $G_S$ is the maximum LEO beam gain, $G_U$ the maximum antenna gain of terrestrial users, $L_{m,k}$ the LSF between the $m$-th LEO satellite and the $k$-th terrestrial user with $L_{m,k} = L(d_{m,k}, f_c; -\eta_1)$, $d_{m,k}$ is the distance between the $m$-th LEO satellite and the $k$-th terrestrial user, and $\eta_1$ is the NLOS path loss coefficient. The elements of $\tilde{\mathbf{g}}_{m,k}$ all conform to the independent complex Gaussian distribution of $\mathcal{CN}(0, 1)$.

For the LOS reflect link, it is divided into two segments: from LEO satellite to the RIS, and from the RIS to terrestrial user. The channel between the $m$-th LEO satellite and the RIS is modelled based on Rician channel model as

$$\mathbf{H}_m = \sqrt{G_S L_{m,R}}\left(\sqrt{\frac{\kappa_1}{\kappa_1+1}}\bar{\mathbf{H}}_m + \sqrt{\frac{1}{\kappa_1+1}}\tilde{\mathbf{H}}_m\right), \tag{3}$$

where $L_{m,R}$ denotes the LSF between $m$-th LEO satellite and RIS with $L_{m,R} = L(d_{m,R}, f_c; -\eta)$, $d_{m,R}$ is the distance between $m$-th LEO satellite and RIS and $\kappa_1$ is the Rician factor of satellite-terrestrial channel. In the Rician channel model, $\bar{\mathbf{H}}_m$ and $\tilde{\mathbf{H}}_m$ denote the LOS and NLOS component respectively. The elements of $\tilde{\mathbf{H}}_m$ are independently chosen from $\mathcal{CN}(0, 1)$. Moreover, $\bar{\mathbf{H}}_m$ is modelled as

$$\begin{aligned}&\bar{\mathbf{H}}_m \\ &= \mathbf{v}_{R_m}(\Psi^x_{AOD,R_m}, \Psi^z_{AOD,R_m})\mathbf{v}^T_{S_m}(\Psi^x_{AOA,S_m}, \Psi^y_{AOA,S_m}),\end{aligned} \tag{4}$$

where $\mathbf{v}_{R_m}$ and $\mathbf{v}_{S_m}$ denote the UPA array response vector of the RIS and the $m$-th LEO satellite respectively, $\Psi^x_{AOA,S_m}$ and $\Psi^y_{AOA,S_m}$ are the angle of arrival (AOA) from LEO satellite to the RIS associated with $x$-axis and $y$-axis respectively, $\Psi^x_{AOD,R_m}$ and $\Psi^z_{AOD,R_m}$ the angle of departure (AOD) from LEO satellite to the RIS associated with $x$-axis and $z$-axis respectively.

Both $\mathbf{v}_{R_m}$ and $\mathbf{v}_{S_m}$ follow similar derivation processes and we take $\mathbf{v}_{S_m}$ as an example. For the UPA array response vector

of the $m$-th LEO satellite, $\mathbf{v}_{S_m} \in \mathbb{C}^{M_S \times 1}$ is deduced by the Kronecker product of the $x$-axis and $y$-axis steering vectors as

$$\mathbf{v}_{S_m} = \mathbf{v}^x_{S_m}(\Psi^x_{AOA,S_m}) \otimes \mathbf{v}^y_{S_m}(\Psi^y_{AOA,S_m}), \tag{5}$$

where $\otimes$ is the Kronecker product, $\mathbf{v}^x_{S_m} \in \mathbb{C}^{M_{S,x} \times 1}$ and $\mathbf{v}^y_{S_m} \in \mathbb{C}^{M_{S,y} \times 1}$ denote the steering vectors of the $x$-axis and $y$-axis respectively. $\mathbf{v}^x_{S_m}(\Psi^x_{AOA,S_m})$ and $\mathbf{v}^y_{S_m}(\Psi^y_{AOA,S_m})$ can be represented as

$$\begin{aligned}&\mathbf{v}^x_{S_m}(\Psi^x_{AOA,S_m}) \\ &= \left[1, e^{-j\pi \sin \Psi^x_{AOA,S_m}}, \ldots, e^{-j\pi(M_{S,x}-1)\sin \Psi^x_{AOA,S_m}}\right]^T,\end{aligned} \tag{6}$$

$$\begin{aligned}&\mathbf{v}^y_{S_m}(\Psi^y_{AOA,S_m}) \\ &= \left[1, e^{-j\pi \sin \Psi^y_{AOA,S_m}}, \ldots, e^{-j\pi(M_{S,y}-1)\sin \Psi^y_{AOA,S_m}}\right]^T.\end{aligned} \tag{7}$$

Based on the 3D spatial configuration, the following equations can be derived regarding the AOA between the $m$-th LEO satellite and the RIS

$$\sin \Psi^x_{AOA,S_m} = \frac{\mathbf{e}_x(\mathbf{r}_{S,m} - \mathbf{r}_R)^T}{|\mathbf{r}_{S,m} - \mathbf{r}_R|}, \tag{8}$$

$$\sin \Psi^y_{AOA,S_m} = \frac{\mathbf{e}_y(\mathbf{r}_{S,m} - \mathbf{r}_R)^T}{|\mathbf{r}_{S,m} - \mathbf{r}_R|}, \tag{9}$$

where $\mathbf{e}_x = [1,0,0]$ and $\mathbf{e}_y = [0,1,0]$ represent the unit vectors in the $x$ and $y$ directions, $\mathbf{r}_{S,m}$ represents the position vector of the $m$-th LEO satellite, and $\mathbf{r}_R$ represents the position vector of the RIS.

Similarly, the channel from the $k$-th user to the RIS $\mathbf{l}_k \in \mathbb{C}^{M_R \times 1}$ is modelled as

$$\mathbf{l}_k = \sqrt{G_U L_{R,k}}\left(\sqrt{\frac{\kappa_2}{\kappa_2+1}}\bar{\mathbf{l}}_k + \sqrt{\frac{1}{\kappa_2+1}}\tilde{\mathbf{l}}_k\right), \tag{10}$$

where $L_{R,k}$ is the LSF between the RIS and the $k$-th terrestrial user with $L_{R,k} = L(d_{R,k}, f_c; -\eta_3)$, $d_{R,k}$ is the distance between the RIS and the $k$-th terrestrial user, $\eta_3$ is the corresponding path loss coefficient, and $\kappa_2$ is the Rician factor of terrestrial channel. Similarly, the elements of NLOS component $\tilde{\mathbf{l}}_k$ are independently selected from $\mathcal{CN}(0,1)$. Meanwhile, $\bar{\mathbf{l}}_k$ denotes the corresponding LOS components represented as

$$\bar{\mathbf{l}}_k = \mathbf{v}^T_{R_k}(\Psi^x_{AOA,R_k}, \Psi^z_{AOA,R_k}), \tag{11}$$

where $\Psi^x_{AOA,R_k}$ and $\Psi^z_{AOA,R_k}$ stand for the AOA from the RIS to the $k$-th terrestrial user associated with $x$-axis and $z$-axis respectively. The derivation process of $\mathbf{v}_{R_k}$ is analogous to that of $\mathbf{v}_{S_m}$.

Under the above analysis, the channel matrix between the $m$-th LEO satellite and the $k$-th terrestrial user is given by

$$\mathbf{h}_{m,k} = \mathbf{l}_k \mathbf{\Psi} \mathbf{H}_m + \mathbf{g}_{m,k}, \tag{12}$$

where $\mathbf{\Psi} = \operatorname{diag}(\Psi_{1,1}, \Psi_{2,2}, \ldots, \Psi_{M_R,M_R})$ represents the RIS phase shift matrix, and $\Psi_{i,i}$ represents the phase shift of the $i$-th reflecting element. The amplification of each RIS reflecting element is set to one for passive RIS in order to ease the implementation of the RIS hardware given by $\|\Psi_{i,i}\|_2 = 1$ for all $i \in [1, M_R]$ and $\Psi_{i,i} = e^{j\phi_i}$ with $\phi_i \in [0, 2\pi)$.

### B. Problem Formulation

To more accurately represent the association between terrestrial users and LEO satellites, a binary user association matrix $\mathbf{A}$, dimensioned $N_S \times N_U$, is employed. Within this matrix, $a_{m,k} = 1$ signifies that the $k$-th terrestrial user access the $m$-th LEO satellite and $a_{m,k} = 0$ otherwise. The signal emitted by the $m$-th LEO satellite is determined as

$$\mathbf{s}_m = \sum_{k=1}^{N_U} \mathbf{w}_{m,k} s_{m,k} a_{m,k}, \tag{13}$$

where $s_{m,k}$ is the signal for the $k$-th terrestrial user by the $m$-th LEO satellite which satisfies $E\left[|s_{m,k}|^2\right] = 1$, and $\mathbf{w}_{m,k} \in \mathbb{C}^{M_S \times 1}\,(1 \le m \le N_S, 1 \le k \le N_U)$ represents the optimization beamforming variable. The overall beamforming matrix of the whole system is denoted as

$$\mathbf{W} = \begin{bmatrix} \mathbf{w}_{1,1} & \mathbf{w}_{1,2} & \cdots & \mathbf{w}_{1,N_U} \\ \mathbf{w}_{2,1} & \mathbf{w}_{2,2} & \cdots & \mathbf{w}_{2,N_U} \\ \vdots & \vdots & \ddots & \vdots \\ \mathbf{w}_{N_S,1} & \mathbf{w}_{N_S,2} & \cdots & \mathbf{w}_{N_S,N_U} \end{bmatrix}. \tag{14}$$

Meanwhile, spatial division multiple access (SDMA) is utilized with proper beamforming, which uses UPA antennas of LEO satellites to spatially separate different users. The SDMA allows multiple terrestrial users to communicate simultaneously on the same frequency channel at the same time. Due to the use of SDMA, each terrestrial user shares the same frequency channel, which inherently leads to co-channel interference between users. Thereby, the signal, $y_{m,k}$, received by the $k$-th terrestrial user sent by the $m$-th LEO satellite combines the desired signal, intra-satellite interference from the same LEO satellite to other users, inter-satellite interference from other LEO satellites and noise which is deduced as

$$\begin{aligned}y_{m,k} = &\underbrace{\mathbf{h}_{m,k}\mathbf{w}_{m,k}s_{m,k}a_{m,k}}_{\text{Desired signal}} + \underbrace{\sum_{k' \ne k} \mathbf{h}_{m,k}\mathbf{w}_{m,k'}s_{m,k'}a_{m,k}x_{m,k'}}_{\text{Intra-satellite interference}} \\ &+ \underbrace{\sum_{m' \ne m}\sum_{k' \ne k} \mathbf{h}_{m',k}\mathbf{w}_{m',k'}s_{m',k'}a_{m,k}a_{m',k'}}_{\text{Inter-satellite interference}} + \underbrace{N_0}_{\text{Noise}},\end{aligned} \tag{15}$$

where $N_0 \sim \mathcal{CN}(0, \sigma_0^2)$ denotes additive Gaussian white noise of power $\sigma_0^2$. The achievable rate of the $m$-th LEO satellite to the $k$-th user is denoted as

$$R_{m,k} = B a_{m,k} \log_2(1 + \gamma_{m,k}), \tag{16}$$

where $B$ is the bandwidth of the frequency channel which is the same for each link, and $\gamma_{m,k}$ is the SINR of data transmitted by the $m$-th LEO satellite to the $k$-th terrestrial user given by

$$\gamma_{m,k} = \frac{|\mathbf{h}_{m,k}\mathbf{w}_{m,k}|^2}{\sum_{m'=1}^{N_S}\sum_{k'=1,k'\ne k}^{N_U} |\mathbf{h}_{m',k}\mathbf{w}_{m',k'}|^2 a_{m,k}a_{m',k'} + \sigma^2}. \tag{17}$$

The sum rate can be derived as

$$R_{SUM} = \sum_{m=1}^{N_S}\sum_{k=1}^{N_U} B a_{m,k} \log_2(1 + \gamma_{m,k}). \tag{18}$$

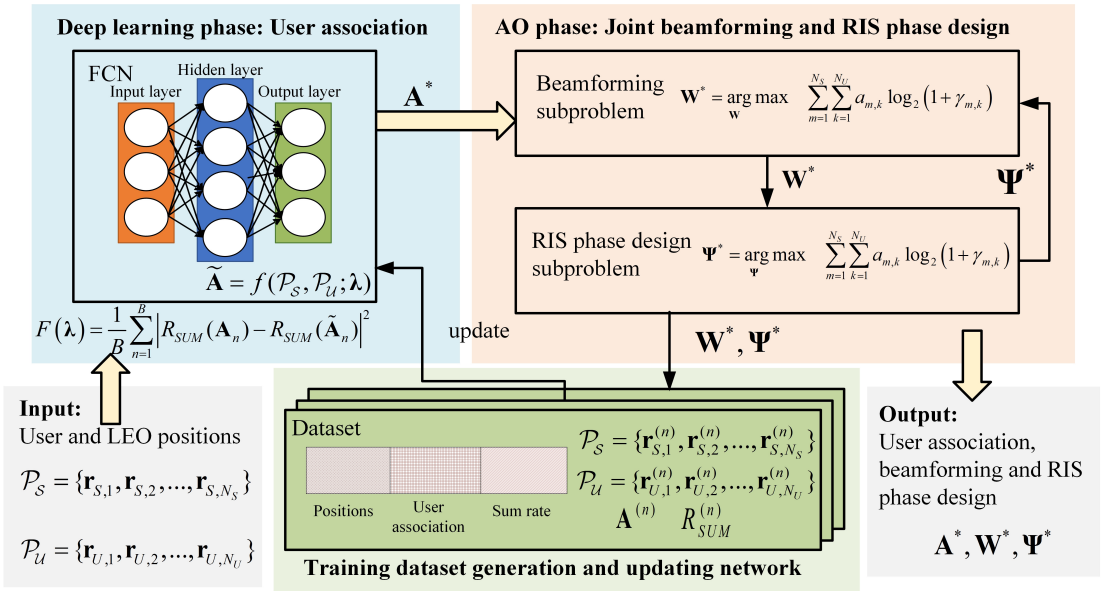


Fig. 2. TPJO for joint user association, beamforming and RIS shift optimization.

We aim to enhance the aggregate downlink sum rate within the given setup through the jointly optimization of the user association matrix, the beamforming at each LEO satellite, and the phase shift of each RIS element. The proposed model is constrained by the rate requirements for each terrestrial user, power transmission limits for each LEO satellite, and user association constraints between LEO satellites and terrestrial users. Consequently, we structure the overarching problem as

$$\max_{\mathbf{W},\mathbf{A},\boldsymbol{\Psi}} \quad \sum_{m=1}^{N_S}\sum_{k=1}^{N_U} a_{m,k}\log_2(1+\gamma_{m,k}) \tag{19a}$$

$$\text{s.t.} \quad \sum_{k=1}^{N_U} a_{m,k}|\mathbf{w}_{m,k}|^2 \le P_0, \quad \forall m \in \mathcal{S}, \tag{19b}$$

$$\sum_{m=1}^{N_S} B a_{m,k}\log_2(1+\gamma_{m,k}) \ge R_0, \quad \forall k \in \mathcal{U}, \tag{19c}$$

$$\sum_{m=1}^{N_S} a_{m,k} = 1, \quad \forall k \in \mathcal{U}, \tag{19d}$$

$$a_{m,k} \in \{0,1\}, \quad \forall m \in \mathcal{S}, k \in \mathcal{U}, \tag{19e}$$

$$|\Psi_{i,i}|^2 = 1, \quad \forall 1 \le i \le M_R, \tag{19f}$$

$$\Psi_{i,i'} = 0, \quad \forall i' \ne i, 1 \le i, i' \le M_R. \tag{19g}$$

In (19), $P_0$ defines the maximum transmission power of LEO satellites with the power constraint presented in (19b), and $R_0 > 0$ specifies the minimum rate of transmission required for every terrestrial user, with its corresponding rate constraint detailed in (19c). It is stipulated that each terrestrial user $k$ is permitted to access only one LEO satellite $m$ within its range, as delineated in (19d) and (19e). Furthermore, the phase limitations for each element of the RIS are outlined in (19f) and (19g), where the RIS phase matrix is a diagonal complex matrix and the Euclidean norm of each diagonal element is 1.

The proposed sum rate maximization model in (19) is an MIP problem which is non-deterministic polynomial-time hard. It is difficult to solve since the objective function and constraints of (19) are all nonconvex. Moreover, the user association, beamforming and RIS phase shifts are coupled both in objective function and constraints which makes the MIP problem much more challenging.

## IV. Algorithm Design

In this section, we design a TPJO algorithm for joint user association, beamforming, and RIS phase design optimization. Specifically, we transform the origin nonconvex problem in (19) into three subproblems of two phases based on DNN and AO, while apply SCA method to transfer the nonconvex problem into convex optimization.

### A. Overview of Proposed TPJO Algorithm

We separate the MIP problem into the programming of integer and continuous variables respectively, and propose a two-phase optimization process for incorporating deep learning and AO. The proposed TPJO algorithm for solving problem (19) is illustrated in Fig. 2 and *Algorithm 1*. In the deep learning phase of integer programming, DNN takes the positions of terrestrial users and LEO satellites as inputs to determine the user association matrix $\mathbf{A}^*$ based on *Algorithm 2*. In the AO phase of continuous programming, the process splits into two subproblems including beamforming and RIS phase design, where the two subproblems are solved iteratively by AO until convergence. To elaborate, we begin the algorithm by initializing the variables $\mathbf{W}^{(0)}$ and $\boldsymbol{\Psi}^{(0)}$. In each subsequent iteration, indexed as $i$, we compute $\mathbf{W}^{(i)}$ and $\boldsymbol{\Psi}^{(i)}$ by solving (34) and (52) based on the solutions obtained in the previous iteration, i.e., $\mathbf{W}^{(i-1)}$ and $\boldsymbol{\Psi}^{(i-1)}$ using *Algorithm 3* and *Algorithm 4* respectively. This iterative process continues until specific convergence criteria are met.

**Algorithm 1** TPJO algorithm.

**Input:** Random initial variables $\mathbf{W}^{(0)}, \mathbf{\Psi}^{(0)}$, threshold $\varepsilon_0$.
**Output:** Solution $\mathbf{A}^*, \mathbf{W}^*, \mathbf{\Psi}^*$.

```
Obtain the user association A* by Algorithm 2.
Obtain the initial sum rate R_SUM^(0) based on A*, W^(0), and Ψ^(0).
Let iteration number i = 0.
repeat
    i = i + 1.
    Update W^(i) by Algorithm 3 based on Ψ^(i-1).
    Update Ψ^(i) by Algorithm 4 based on W^(i-1).
    Obtain R_SUM^(i) by A*, W^(i), and Ψ^(i).
until |R_SUM^(i) − R_SUM^(i-1)| < ε_0.
W* = W^(i).
Ψ* = Ψ^(i).
return A*, W*, Ψ*.
```

### *B. Deep Learning Phase for User Association*

By fixing the beamforming matrix $\mathbf{W}$ and RIS phase shift $\mathbf{\Psi}$, the original optimization problem (19) is transferred into the user association optimization subproblem of $\mathbf{A}$ which can be formulated as

$$\max_{\mathbf{A}} \quad \sum_{m=1}^{N_S}\sum_{k=1}^{N_U} a_{m,k}\log_2\left(1+\gamma_{m,k}\right) \tag{20}$$
$$\text{s.t.} \quad \text{(19b)} - \text{(19e)}.$$

Conventional algorithms for user association, such as many-to-one matching or optimization-based approaches, require substantial computation after acquiring user and satellite positions, leading to increased latency, especially in high-mobility LEO satellite environments. In contrast, using DNN algorithm allows for real-time prediction of user associations by training offline on simulated possible future positions, making it a more efficient and latency-sensitive solution. Here, we focus on leveraging the power of deep learning algorithms to establish a comprehensive understanding of the relationships among user positions, LEO satellite positions, and user association in (20).

*1) Training dataset construction*

We generate the training dataset for DNN using data samples including user positions, satellite positions and user association schemes, as shown in Fig. 2. Specifically, we first generate user positions considering the uniform random distribution of users. Then satellite positions are generated randomly of possible satellite positions of certain orbit parameters. Let $\mathcal{P}_\mathcal{S} = \{\mathbf{r}_{S,1}, \mathbf{r}_{S,2}, ..., \mathbf{r}_{S,N_S}\}$ and $\mathcal{P}_\mathcal{U} = \{\mathbf{r}_{U,1}, \mathbf{r}_{U,2}, ..., \mathbf{r}_{U,N_U}\}$ denote the position sets of LEO satellites and terrestrial users respectively. For each position set pair of user and satellite positions $(\mathcal{P}_\mathcal{S}, \mathcal{P}_\mathcal{U})$, we generate we generate user association scheme from maximum remaining time access [27], and $\mu$ random access schemes, where Monte Carlo method is used. Among these $\mu+1$ schemes, the scheme with the highest sum rate value calculated by *Algorithm 3* and *Algorithm 4* in AO phase is chosen to form the dataset.

The $n$-th training sample in the dataset is given by

$$\left\{ \underbrace{\mathbf{r}_{S,1}^{(n)}, \ldots, \mathbf{r}_{S,N_S}^{(n)}}_{\text{LEO positions}}, \underbrace{\mathbf{r}_{U,1}^{(n)}, \ldots, \mathbf{r}_{U,N_U}^{(n)}}_{\text{user positions}}, \underbrace{\mathbf{A}^{(n)}}_{\substack{\text{user}\\ \text{association}}}, \underbrace{R_{\text{SUM}}^{(n)}}_{\substack{\text{maximum}\\ \text{sum rate}}} \right\}.$$

Here, $\mathbf{r}_{S,m}$, $\mathbf{r}_{U,k}$ denote the normalized position input of LEO position and user position, respectively, where $1 \le m \le M$ and $1 \le k \le K$. Notably, the RIS position is not used as an input here, as RISs are typically deployed on the exterior surfaces of buildings, and their positions remain fixed after deployment. When considering RIS deployment locations, we can train different FCNN models for each specific position. The DNN is tasked to learn the complex interplay between terrestrial user and LEO satellite positions, and their direct impact on the establishment of reliable and efficient communication links, ultimately contributing to the optimization of network performance in terms of the sum rate.

*2) DNN with FCNN architecture*

We utilize an FCNN architecture of DNN with three hidden layers to approximate the optimal user association solution of (20). The relationship between LEO positions $\mathcal{P}_\mathcal{S}$, user positions $\mathcal{P}_\mathcal{U}$ and user association matrix $\mathbf{A}$ is expressed as

$$\tilde{\mathbf{A}} = f(\mathcal{P}_\mathcal{S}, \mathcal{P}_\mathcal{U}; \boldsymbol{\lambda}). \tag{21}$$

Here, $f(\cdot)$ denotes FCNN architecture with parameters $\boldsymbol{\lambda}$ based on the rectified linear unit (ReLU) function. The output $\tilde{\mathbf{A}}$ predicted by the DNN consists of continuous variables. To convert $\tilde{\mathbf{A}}$ into a binary user association matrix $\mathbf{A}$, we associate each terrestrial user with the LEO satellite corresponding to the maximum value in $\tilde{\mathbf{A}}$. For the discretization of $\tilde{\mathbf{A}}$, we define that the maximum element in each column is set to one, while the others are set to zero. The output of the DNN is represented as $\mathbf{A}$.

*3) Training Procedure*

The FCNN parameter, $\boldsymbol{\lambda}$, is updated by minimizing the loss function embedded in the sum rate of ULSNs in each training step. The loss function is calculated by the mean squared error (MSE) [28] which measures the difference between sum rate $R_{SUM}(\mathbf{A})$ computed with the current association matrix $\mathbf{A}$ and sum rate $R_{SUM}(\tilde{\mathbf{A}})$ obtained with the predicted association matrix $\tilde{\mathbf{A}}$ by (21) defined as

$$F(\boldsymbol{\lambda}) = \frac{1}{D}\sum_{n=1}^{D}\left|R_{SUM}(\mathbf{A}_n) - R_{SUM}(\tilde{\mathbf{A}}_n)\right|^2, \tag{22}$$

where $D$ represents the batch size in the FCNN, and $\mathbf{A}_n$ denotes the user association matrix in the $n$-th batch. As outlined in *Algorithm 3*, the LEO satellite positions $\mathcal{P}_\mathcal{S}{}^{(n)} = \{\mathbf{r}_{S,1}^{(n)}, \mathbf{r}_{S,2}^{(n)}, ..., \mathbf{r}_{S,N_S}^{(n)}\}$, user positions $\mathcal{P}_\mathcal{U}{}^{(n)} = \{\mathbf{r}_{U,1}^{(n)}, \mathbf{r}_{U,2}^{(n)}, ..., \mathbf{r}_{U,N_U}^{(n)}\}$, user association matrix $\tilde{\mathbf{A}}^{(n)}$, and the corresponding sum rate $R_{SUM}^{(n)}$ are stored in the training buffer of the DNN. After calculating the MSE, $\boldsymbol{\lambda}$ is updated to minimize this error. This step is repeated for each training iteration, progressively refining the DNN's ability to predict the user association matrix.

**Algorithm 2** DNN based user association.

**Input:** The buffer $\mathcal{B} = \{\mathcal{B}_1, \mathcal{B}_2, ..., \mathcal{B}_{N_{sample}}\}$ with $N_{sample}$ sets of positions of users $\mathcal{U}$ and LEO satellites $\mathcal{S}$.

**Output:** A final user association matrix $\mathbf{A}^*$ between terrestrial users $\mathcal{U}$ and LEO satellites $\mathcal{S}$.

*Offline Training:*
**for** each training step **do**
  Calculate the MSE $F(\boldsymbol{\lambda}) = \frac{1}{D}\sum_{n=1}^{D}\left|R_{SUM}(\mathbf{A}_n) - R_{SUM}(\tilde{\mathbf{A}}_n)\right|^2$.
  Updating the network parameter $\boldsymbol{\lambda}$.
**end for**
Store the FCNN parameter $\boldsymbol{\lambda}$.
*On-line Stage:*
Calculating the user association matrix $\tilde{\mathbf{A}}$ according to the trained FCNN as $\tilde{\mathbf{A}} = f(\mathcal{P}_{\mathcal{S}}, \mathcal{P}_{\mathcal{U}}; \boldsymbol{\lambda})$.
Set the maximum value of each column of $\tilde{\mathbf{A}}$ as 1 and others as 0.
**return** Final user association matrix $\mathbf{A}^*$ between terrestrial users $\mathcal{U}$ and LEO satellites $\mathcal{S}$.

*4) User association scheme*

Then, in the online stage, user association matrix $\hat{\mathbf{A}}$ is computed using the fully trained DNN. This calculation is based on the current positions of the LEO satellites, $\mathcal{P}_S$, and the terrestrial users, $\mathcal{P}_U$, along with the stored parameters $\boldsymbol{\lambda}$, which were optimized during the offline training stage. Once association matrix $\hat{\mathbf{A}}$ is calculated, the algorithm performs a post-processing step to optimal user association matrix $\mathbf{A}^*$ based on aforementioned discretization method.

### C. Beamforming Optimization in AO Phase

After determining the user association $\mathbf{A}^*$ through DNN in the deep learning phase, the original MIP problem becomes a continuous optimization problem concerning beamforming and RIS phase design. Then in AO phase, the continuous optimization problem can be reduced into beamforming optimization subproblem for given RIS phase matrix $\boldsymbol{\Psi}$ which is denoted as

$$\max_{\mathbf{W}} \quad \sum_{m=1}^{N_S}\sum_{k=1}^{N_U} a_{m,k}\log_2(1+\gamma_{m,k}) \tag{23a}$$
$$\text{s.t.} \quad \text{(19b) and (19c).}$$

Constraint (19b) is convex, while the objective function in (23a) and constraint (19c) are nonconvex which can be transformed into convex by applying approximations that render their tractability.

Given the characteristics of user association $\mathbf{A}$ that each user is able to access only one satellite, we can define auxiliary variable $t_k (1 \le k \le N_U)$ for user $k$ and have equivalent transformations of the original problem. Specifically, the auxiliary variable $t_k$ is expressed as

$$t_k = \sum_{m=1}^{N_S} a_{m,k}\gamma_{m,k} + 1. \tag{24}$$

For $\forall k \in \mathcal{U}$, there is only one $m \in \mathcal{S}$ satisfy $a_{m,k} = 1$. Assuming that $a_{m,k} = 1$ for user $k$, $t_k = \gamma_{m,k} + 1$. Accordingly, beamforming subproblem (23) can be transformed into equivalent form as follows

$$\max_{\mathbf{W}, t_k} \quad \sum_{k=1}^{N_U}\log_2 t_k \tag{25a}$$
$$\text{s.t.} \quad \text{(19b), (19c) and (24).}$$

Combining constraints (19b) and (24) with the fractional equation (17), constraint (19b) is reformulated into (26) and (27) by incorporating auxiliary slack variable $\beta_k > 0$ for $\forall k \in \mathcal{U}$ [29],

$$\sum_{m=1}^{N_S} a_{m,k}|\mathbf{h}_{m,k}\mathbf{w}_{m,k}| \ge \beta_k\sqrt{t_k - 1}, \tag{26}$$

$$\sum_{m=1}^{N_S} a_{m,k}\sum_{m'=1}^{N_S}\sum_{k'=1,k'\neq k}^{N_U} a_{m',k'}\left|\mathbf{h}_{m',k}\mathbf{w}_{m',k'}\right|^2 + \sigma^2 \le \beta_k^2. \tag{27}$$

Constraint (27) is convex, while the right side of the inequality (26) is quasi-concave which is still non-convex. SCA algorithm is usually employed to iteratively approximate and solve non-convex problems by constructing a sequence of convex subproblems. In this paper, we use SCA to approximate the constraint (26) by its convex upper bound in each iteration of SCA. Since (26) is nonconvex for the defined domain where $\beta_k > 0$ and $t_k > 1$, we denote function $g(\beta_k, t_k)$ as

$$g(\beta_k, t_k) = \beta_k\sqrt{t_k - 1}, \tag{28}$$

where $\beta_k > 0$ and $t_k > 1$. Function $h(\beta_k, t_k; \delta_k)$ can be written as

$$h(\beta_k, t_k; \delta_k) = \frac{\delta_k}{2}\beta_k^2 + \frac{1}{2\delta_k}(t_k - 1). \tag{29}$$

According to the characteristic of arithmetic and geometric means, the following inequality holds for all $\delta_k > 0$

$$\beta_k\sqrt{t_k - 1} \le \frac{\delta_k}{2}\beta_k^2 + \frac{1}{2\delta_k}(t_k - 1). \tag{30}$$

Then, $h(\beta_k, t_k; \delta_k)$ is always an upper bound on $g(\beta_k, t_k)$ and $h(\beta_k, t_k; \delta_k) \ge g(\beta_k, t_k)$. Moreover, when fixed point $\delta_k = \sqrt{t_k - 1}/\beta_k$ is reached, the following equalities hold

$$h(\beta_k, t_k; \delta_k) = g(\beta_k, t_k), \tag{31}$$

$$\nabla h(\beta_k, t_k; \delta_k) = \nabla g(\beta_k, t_k), \tag{32}$$

where $\nabla h(\beta_k, t_k; \delta_k)$ and $\nabla g(\beta_k, t_k)$ are the gradients of the functions $h(\beta_k, t_k; \delta_k)$ and $g(\beta_k, t_k)$ respectively. Obviously, $h(\beta_k, t_k; \delta_k)$ is convex and (26) is restricted into

$$\sum_{m=1}^{N_S} a_{m,k}|\mathbf{h}_{m,k}\mathbf{w}_{m,k}| \ge \frac{\psi_k}{2}\beta_k^2 + \frac{t_k - 1}{2\psi_k}. \tag{33}$$

**Algorithm 3** SCA based beamforming optimization.

**Input:** Initial beamforming matrix $\mathbf{W}^{(0)}$, threshold $\varepsilon_1$.
**Output:** Optimal $\mathbf{W}^*$.

$i = 0$.
Initialize $\delta_k^{(i)}$ at random.
**repeat**
  Solve (34) with $\delta_k^{(i)}$ using CVX and get the optimal $\left(t_k^{(i)}, \beta_k^{(i)}, \mathbf{W}^{(i)}\right)$ with sum rate of $R_{SUM}^{(i)}$.
  Update $\mathbf{W}^* = \mathbf{W}^{(i)}$.
  Update $\delta_k^{(i+1)} = \sqrt{t_k^{(i)} - 1}/\beta_k^{(i)}$.
  Update $\Delta R_{SUM} = R_{SUM}^{(i)} - R_{SUM}^{(i-1)}$.
  $i = i + 1$.
**until** $\Delta R_{SUM}$ below a threshold $\varepsilon_2 > 0$.
**return** Optimal beamforming $\mathbf{W}^*$.

Based on SCA, the quasi-concave inequality is replaced by it upper bound and problem (25) is transferred into

$$\max_{\mathbf{W}, t_k, \beta_k} \quad \sum_{k=1}^{N_U} \log_2 t_k \tag{34a}$$

$$\text{s.t.} \quad \sum_{k=1}^{N_U} a_{m,k} |\mathbf{w}_{m,k}|^2 \le P_0, \quad \forall m \in \mathcal{S}, \tag{34b}$$

$$t_k \ge 2^{R_0/B}, \quad \forall k \in \mathcal{U}, \tag{34c}$$

$$t_k \ge 1, \quad \forall k \in \mathcal{U}, \tag{34d}$$

$$\beta_k > 0, \quad \forall k \in \mathcal{U}, \tag{34e}$$

(33) and (27).

It is noted that, for each iteration, problem (34) is transferred into a convex second order cone problem (SOCP). Specifically, SOCP can be solved using Mosek which is an efficient CVX solver for SOCP. At each iteration, $\delta_k$ is updated by its fixed point in (30) using the optimal $\beta_k$ and $t_k$ in the previous iteration. $\delta_k$ is updated as

$$\delta_k^{(i)} = \sqrt{t_k^{(i-1)} - 1}/\beta_k^{(i-1)}. \tag{35}$$

*Algorithm 3* shows the detailed SCA based beamforming algorithm for subproblem (34).

### *D. RIS Phase Shift Optimization in AO Phase*

In the AO phase, the RIS shift phase optimization subproblem for a given beamforming matrix $\mathbf{W}$ is formulated as

$$\max_{\mathbf{\Psi}} \quad \sum_{m=1}^{N_S} \sum_{k=1}^{N_U} a_{m,k} \log_2 (1 + \gamma_{m,k}) \tag{36a}$$

$$\text{s.t.} \quad \text{(19c), (19f) and (19g).}$$

Although constraints (19f) and (19g) are convex, subproblem (36) remains non-convex in terms of the RIS phase matrix $\mathbf{\Psi}$ embedded in the sum rate expression which is nonconvex.

To make the RIS phase design subproblem (36) tractable, we decouple the original channel into the direct link which does not contain the RIS phase matrix $\mathbf{\Psi}$ and the RIS link which contains the RIS phase matrix $\mathbf{\Psi}$. These two parts can be transferred into effective links as $\mathbf{a}_{k,k'}$ and $\mathbf{b}_{k,k'}$, respectively. The effective links $\mathbf{a}_{k,k'}$ and $\mathbf{b}_{k,k'}$ are defined as

$$\mathbf{a}_{k,k'} = \sum_{m=1}^{N_S} \sum_{m'=1}^{N_S} \text{diag}\left(\mathbf{l}_{m',k}\right) \mathbf{\Psi} a_{m,k} \cdot \mathbf{w}_{m',k'} a_{m',k'}, \tag{37}$$

$$\mathbf{b}_{k,k'} = \sum_{m=1}^{N_S} \sum_{m'=1}^{N_S} \mathbf{g}_{m',k} a_{m,k} \cdot \mathbf{w}_{m',k'} a_{m',k'}. \tag{38}$$

*Proposition 1:* The data rate of the $k$-th user $R_k$ can be represented by effective channels $\mathbf{a}_{k,k'}$ and $\mathbf{b}_{k,k'}$ as

$$R_k = B \log \left(1 + \frac{\left|\mathbf{u}^H \mathbf{a}_{k,k} + \mathbf{b}_{k,k}\right|^2}{\sum_{k'=1, k' \ne k}^{N_U} \left|\mathbf{u}^H \mathbf{a}_{k,k'} + \mathbf{b}_{k,k'}\right|^2 + \sigma^2}\right), \tag{39}$$

where $\mathbf{u} = [\Psi_{1,1}, \Psi_{2,2}, \ldots, \Psi_{M_R,M_R}]$.

*Proof :* Considering the constraints that each terrestrial user is capable to access one LEO satellite within coverage at each time. For $\forall k \in \mathcal{U}$, there is only one $m \in \mathcal{S}$ satisfy $a_{m,k} = 1$. For user $k$ and user $k'$, assuming $a_{m,k} = 1$ and $a_{m',k'} = 1$ then received data rate of the $k$-th user is represented as

$$R_k = B \log (1 + \gamma_{m,k}). \tag{40}$$

In this case, $\mathbf{a}_{k,k'}$ and $\mathbf{b}_{k,k'}$ can be expressed as $\mathbf{a}_{k,k'} = \text{diag}\left(\mathbf{l}_{m,k}\right) \mathbf{\Psi} \mathbf{w}_{m',k'}$ and $\mathbf{b}_{k,k'} = \mathbf{g}_{m,k} \mathbf{w}_{m',k'}$.

The power of expected signal received by the $k$-th terrestrial user is derived as

$$\begin{aligned} |\mathbf{h}_{m,k} \mathbf{w}_{m,k}|^2 &= \left|\text{diag}\left(\mathbf{l}_{m,k}\right) \mathbf{\Psi} \mathbf{w}_{m,k} + \mathbf{g}_{m,k} \mathbf{w}_{m,k}\right|^2 \\ &= \left|\mathbf{u}^H \mathbf{a}_{k,k} + \mathbf{b}_{k,k}\right|^2. \end{aligned} \tag{41}$$

Meanwhile, the power of interference signal received by the $k$-th user is derived as

$$\begin{aligned} &\sum_{m'=1}^{N_S} \sum_{k'=1, k' \ne k}^{N_U} a_{m',k'} \left|\mathbf{h}_{m',k} \mathbf{w}_{m',k'}\right|^2 \\ &= \sum_{m'=1}^{N_S} \sum_{k'=1, k' \ne k}^{N_U} a_{m',k'} \left|\text{diag}\left(\mathbf{l}_{m',k}\right) \mathbf{\Psi} \mathbf{w}_{m',k'} + \mathbf{g}_{m',k} \mathbf{w}_{m',k'}\right|^2 \\ &= \sum_{k' \ne k} \left|\mathbf{u}^H \mathbf{a}_{k,k'} + \mathbf{b}_{k,k'}\right|^2. \end{aligned} \tag{42}$$

Substituting equations (41) and (42) into (40) gives the proof to obtain (39) where the transmission rate is expressed by effective channels. ■

Due to the complex non-convex interactions between user interference and phase shift variables, we use the SCA method to approximate the problem as a convex one, ensuring a tractable solution within a reasonable time for ULSN applications. Similarly, we then introduce auxiliary variable $\chi_k$ where $1 \le k \le K$ and

$$\chi_k = 1 + \frac{\left|\mathbf{u}^H \mathbf{a}_{k,k} + \mathbf{b}_{k,k}\right|^2}{\sum_{k'=1, k' \ne k}^{N_U} \left|\mathbf{u}^H \mathbf{a}_{k,k'} + \mathbf{b}_{k,k'}\right|^2 + \sigma^2}. \tag{43}$$

Following monotonicity of logarithmic function, the original RIS phase subproblem in (36) is reduced to

$$\max_{\chi_k,\mathbf{u}} \quad \sum_{k=1}^{N_U} \log_2 \chi_k \tag{44a}$$

$$\text{s.t.} \quad \left|\mathbf{u}^H\mathbf{a}_{k,k}+\mathbf{b}_{k,k}\right|^2 \geq \left(2^{R_0/B}-1\right)\left(\sum_{k'=1,k'\neq k}^{N_U}\left|\mathbf{u}^H\mathbf{a}_{k,k'}+\mathbf{b}_{k,k'}\right|^2+\sigma^2\right), \tag{44b}$$

$$|\mathbf{u}_n|^2=1, \tag{44c}$$

$$\chi_k = 1+\frac{\left|\mathbf{u}^H\mathbf{a}_{k,k}+\mathbf{b}_{k,k}\right|^2}{\sum_{k'=1,k'\neq k}^{N_U}\left|\mathbf{u}^H\mathbf{a}_{k,k'}+\mathbf{b}_{k,k'}\right|^2+\sigma^2}. \tag{44d}$$

Introduce auxiliary variable $\mathbf{R}_{k,j}$ and $\mathbf{U}$ [31] where

$$\mathbf{R}_{k,j}=\begin{bmatrix}\mathbf{a}_{k,j}\mathbf{a}_{k,j}^H & \mathbf{a}_{k,j}\mathbf{b}_{k,j}^H\\ \mathbf{a}_{k,j}^H\mathbf{b}_{k,j} & 0\end{bmatrix}, \tag{45}$$

$$\mathbf{U}=\begin{bmatrix}\mathbf{u}\mathbf{u}^H & \mathbf{u}^H\\ \mathbf{u} & 1\end{bmatrix}. \tag{46}$$

Note that $\mathbf{U}$ can be expressed as $\mathbf{U}=[\mathbf{u}\quad 1][\mathbf{u}\quad 1]^H$ which is positive definite and of rank 1 satisfying $\mathbf{U}\succeq 0$ and $\text{rank}(\mathbf{U})=1$. The power of desired signal can be converted as follow

$$\begin{aligned}\left|\mathbf{u}^H\mathbf{a}_{k,k}+\mathbf{b}_{k,k}\right|^2 &= \mathbf{u}^H\mathbf{a}_{k,k}\mathbf{a}_{k,k}^H\mathbf{u}+\mathbf{u}^H\mathbf{a}_{k,k}\mathbf{b}_{k,k}^H\\ &\quad+\mathbf{b}_{k,k}\mathbf{a}_{k,k}^H\mathbf{u}+|\mathbf{b}_{k,k}|^2\\ &= \text{tr}\left(\mathbf{R}_{k,k}\mathbf{U}\right)+|\mathbf{b}_{k,k}|^2.\end{aligned} \tag{47}$$

Similarly to the method in solving (23) by introducing additional slack variables variable $\alpha_k>0$, we can change the nonconvex constraint (44b) into two convex constraints and solved by SCA iteratively:

$$\text{tr}\left(\mathbf{R}_{k,k}\mathbf{U}\right)+|\mathbf{b}_{k,k}|^2\geq\alpha_k^2(\chi_k-1), \tag{48}$$

$$\sigma^2+\sum_{k'=1,k'\neq k}^{N_U}\left(\text{tr}\left(\mathbf{R}_{k,k'}\mathbf{U}\right)+|\mathbf{b}_{k,k'}|^2\right)\leq\alpha_k^2. \tag{49}$$

Nonconvex constraint (48) has convex upper bound

$$y(\alpha_k,\chi_k;\psi_k)=\frac{\psi_k\alpha_k^4}{2}+\frac{(\chi_k-1)^2}{2\psi_k}. \tag{50}$$

Then (48) can be restricted into convex constraint as

$$\text{tr}\left(\mathbf{R}_{k,k}\mathbf{U}\right)+|\mathbf{b}_{k,k}|^2\geq\frac{\psi_k\alpha_k^4}{2}+\frac{(\chi_k-1)^2}{2\psi_k}. \tag{51}$$

In each iteration, we relax the rank-one constraint and using SCA to transform the original nonconvex subproblem of RIS phase design into a series of convex subproblems solved iteratively. Then, problem (36) is transformed to

$$\max_{\alpha_k,\chi_k,\mathbf{U}} \quad \sum_{k=1}^{N_U}\log_2\chi_k \tag{52a}$$

$$\text{s.t.} \quad \mathbf{U}_{n,n}=1,\quad \forall 1\leq n\leq M_R, \tag{52b}$$

$$\mathbf{U}\succeq 0, \tag{52c}$$

$$\chi_k\geq 2^{R_0/B},\quad \forall k\in\mathcal{U}, \tag{52d}$$

$$\chi_k\geq 1,\quad \forall k\in\mathcal{U}, \tag{52e}$$

$$\alpha_k>0,\quad \forall k\in\mathcal{U}, \tag{52f}$$

(51) and (48).

Problem (52) is equivalent to problem (44) solely when the optimal solution, denoted as $\mathbf{U}$, maintains a rank-one structure and is positive semidefinite. Nonetheless, the optimal rank for problem (52) might exceed one since the rank-one restriction has been relaxed. At this time, the sum rate achieved by optimal solution of problem (52) is just an upper bound of the problem (44). similarly, at each iteration $\delta_k$ is updated by its fixed point in (30) as

$$\psi_k^{(i)}=\left(\chi_k^{(i-1)}-1\right)/\left(\alpha_k^{(i-1)}\right)^2. \tag{53}$$

To approach the upper bound of the original problem, the Gaussian randomization method [32] is employed to generate a rank-one positive semidefinite matrix from the higher-rank solution $\mathbf{U}$. The proposed SCA and Gaussian randomization

**Algorithm 4** SCA and Gaussian randomization based RIS phase optimization.

**Input:** Initial RIS phase $\mathbf{\Psi}^{(0)}$, threshold $\varepsilon_2$.
**Output:** Optimal $\mathbf{\Psi}^*$.

$i=0$.
Initialize $\delta_k^{(i)}$ at random.
**repeat**
  Solve (34) with $\delta_k^{(i)}$ using CVX and get the optimal solution of $\left(t_k^{(i)},\beta_k^{(i)},\mathbf{U}^{(i)}\right)$ with sum rate of $R_{SUM}^{(i)}$.
  Update $\mathbf{V}^*=\mathbf{U}^{(i)}$.
  Update $\delta_k^{(i+1)}=\left(t_k^{(i)}-1\right)/\beta_k^2(i)$.
  Update $\Delta R_{SUM}=R_{SUM}^{(i)}-R_{SUM}^{(i-1)}$.
  $i=i+1$.
**until** $\Delta R_{SUM}$ below a threshold $\varepsilon_3>0$.
Calculate the diagonal matrix $\mathbf{D}$ of eigenvalues and the corresponding matrix $\mathbf{V}$ combined of right eigenvectors.
**if** $\text{rank}(\mathbf{U}^*)=1$ **then**
  $\mathbf{u}=\boldsymbol{V}\sqrt{\boldsymbol{D}}$.
  $\mathbf{\Psi}^*=\text{diag}\{e^{j\arg\frac{\mathbf{u}[1]}{\mathbf{u}[M_R+1]}},\cdots,e^{j\arg\frac{\mathbf{u}[M_R]}{\mathbf{u}[M_R+1]}}\}$.
**else**
  **for** $m=1,2,\cdots,M$ **do**
    calculate $\mathbf{\Psi}_m$ according to (56) of sum rate $R_{SUM}^m$.
  **end for**
  $m^*=\arg\max_m R_{SUM}^m$.
  $\mathbf{\Psi}^*=\mathbf{\Psi}_{m^*}$.
**end if**
**return** $\mathbf{\Psi}^*$.

based RIS phase optimization is summarized in *Algorithm 3*. We initiate the process by computing the diagonal matrix $\mathbf{D}$ containing eigenvalues and the associated matrix $\mathbf{V}$, comprising right eigenvectors. This is achieved through eigenvalue decomposition as follows:

$$\mathbf{U} = \mathbf{V}^H \mathbf{D} \mathbf{V}. \tag{54}$$

where $\mathbf{D} = [\lambda_1, ..., \lambda_{M_R}]$ is diagonal matrix composed of eigenvalues of $\mathbf{U}$ and $\mathbf{V} = [\mathbf{e}_1, ..., \mathbf{e}_{M_R}]$ consists of corresponding eigenvectors of $\mathbf{U}$.

We generate $M$ candidate vectors based on the Gaussian randomization method as follows

$$\tilde{\mathbf{u}}_m = \mathbf{V}^H \mathbf{D}^{\frac{1}{2}} \mathbf{r}_m, \quad m = 1, 2 \cdots, M, \tag{55}$$

where $\mathbf{V}$ is a unitary matrix consisting of the right eigenvectors, $\mathbf{D}$ is a diagonal matrix containing the eigenvalues, and $\mathbf{r}_m$ represents a random vector. The elements of the vector $\mathbf{r}_m$ are mutually independent distributed random variables with Euclidean norm of 1. Using $\tilde{\mathbf{u}}_m$, the candidate RIS phase shift matrix are

$$\tilde{\mathbf{\Psi}}_m = \mathrm{diag}\left\{ e^{j \arg \frac{\tilde{\mathbf{u}}_m[1]}{\tilde{\mathbf{u}}_m[M_R+1]}}, \cdots, e^{j \arg \frac{\tilde{\mathbf{u}}_m[M_R]}{\tilde{\mathbf{u}}_m[M_R+1]}} \right\}. \tag{56}$$

The optimal RIS phase shift matrix $\mathbf{\Psi}^*$ is chosen from $\left\{ \tilde{\mathbf{\Psi}}_1, \tilde{\mathbf{\Psi}}_2, \cdots, \tilde{\mathbf{\Psi}}_M \right\}$ which maximizes the sum rate and satisfies all the constraints of problem (52).

### *E. Convergence and Complexity Analysis*

In the AO phase, the original problem is transformed into two subproblems, denoted as (23) and (36), as discussed in the previous section. These subproblems handle different optimization variables and are solved iteratively. The AO joint beamforming and RIS phase shift optimization method demonstrates provable convergence under certain conditions.

*Proposition 2:* The value of sum rate in (19) is non-increasing over the iterations following *Algorithm 4*.

*Proof:* Define the objective function in (19) as $G(\mathbf{W}, \mathbf{\Psi})$ corresponding to certain beamforming $\mathbf{W}$ and RIS phase shift $\mathbf{\Psi}$. Since the objective function is the same in (23) and (36), expression holds that

$$G(\mathbf{W}^{i-1}, \mathbf{\Psi}^{i-1}) \leq G(\mathbf{W}^{i}, \mathbf{\Psi}^{i-1}) \leq G(\mathbf{W}^{i}, \mathbf{\Psi}^{i}). \tag{57}$$

As shown in steps 3 and 4 in *Algorithm 1*, if there exists a feasible solution to (36), it is also feasible to (23). This means that for fix RIS phase shift $\mathbf{\Psi}^{i-1}$, both $(\mathbf{W}^{i-1}, \mathbf{\Psi}^{i-1})$ and $(\mathbf{W}^{i}, \mathbf{\Psi}^{i-1})$ are feasible solutions while $(\mathbf{W}^{i}, \mathbf{\Psi}^{i-1})$ is the optimal. Nevertheless $F(\mathbf{W}^{i-1}, \mathbf{\Psi}^{i-1}) \leq G(\mathbf{W}^{i}, \mathbf{\Psi}^{i-1})$ holds and (57) can be proved in similar manner. ■

To evaluate the effectiveness of the proposed algorithms, we analyze their computational complexity. This analysis helps understand the algorithms' performance and feasibility for practical applications in ULSN. The computational complexity of both *Algorithm 3* and *Algorithm 4* depends on the number of iterations, and the number and size of optimization variables and constraints [33]. For the beamforming subproblem solved by *Algorithm 3*, the convex problem (34) has $2N_SN_U + N_SN_UM_S$ variables, $3N_U$ linear constraints, and $2N_U + N_S$ second order cone (SOC) constraints. Thus, the complexity $\tau_1$ of *Algorithm 3* is shown in (58), and $n_1 = (2N_SN_U + N_SN_UM_S)$. For the RIS phase subproblem solved by *Algorithm 4*, the convex problem (52) has $M_R^2 + 2N_S$ design variables, $3N_U + M_R$ linear constraints of size 1, $2N_U$ SOC constraints of size 1 and 1 SOC constraints of size $M_R + 1$. Similarly, the complexity $\tau_2$ of *Algorithm 4* is shown in (59), and $n_2 = (M_R^2 + 2N_S)$. And the complexity of AO procedure in *Algorithm 1* can be calculated based on the complexity of *Algorithm 3* and *Algorithm 4* as $O\left(\ln(1/\varepsilon_0)(\tau_1 + \tau_2)\right)$.

TABLE I
MAIN SIMULATION PARAMETERS

| Parameters | Values |
|---|---|
| Rician factors $\kappa_1$ and $\kappa_2$ | 15, 10 dB |
| Frequency band $f_c$ | 150 MHz [15] |
| Power density of Gaussian white noise $N_0$ | -204 dBm/Hz |
| Number of LEO satellite antennas $M_0$ | 4∼16 |
| Bandwidth of each LEO satellite link $B$ | 20 MHz [36] |
| Maximum LEO accessibility evaluation angle | 45° [1] |
| Transmission power for each LEO satellite $P_0$ | 30∼50 dBm [37] |
| Maximum beam gain of each LEO satellite $G_S$ | 50dBi [17] |
| Maximum antenna gain of each terrestrial user $G_U$ | 20dBi |
| Thresholds $\varepsilon_0$, $\varepsilon_2$ and $\varepsilon_3$ | $10^{-2}$ |
| Training threshold of DNN $\varepsilon_1$ | $10^{-5}$ |

## V. SIMULATION

In this section, we evaluate the performance of the proposed TPJO algorithm through numerical assessment. Terrestrial users are deployed in a circle centred at $(0\ \mathrm{m}, 50\ \mathrm{m}, r_e)$ with radius of 50m where $r_e$ is the radius of the earth. Based on the analysis presented in [34], the sum rate performance of ULSN is similar when there are five or more satellites available for each user. Therefore, we set $N_S = 5$, where these satellites are at lower orbital altitudes ranging from 500 km to 550 km chosen from Starlink constellation with 11,927 satellites [35]. And Table I encapsulates the main simulation parameters vital for the assessment of the proposed algorithms.

To demonstrate the enhanced performance of the proposed TPJO algorithm and to elucidate the simulation, we assess its effectiveness against these baseline algorithms:

- RIS with random phase (RP-RIS): The phase of each diagnal element of $\mathbf{\Psi}$ is initialized by random value from 0 to $2\pi$. Meanwhile, user association and beamforming are solved by *Algorithm 2* and *Algorithm 3*, respectively.

$$\tau_1 = O\left(\sqrt{7N_U + 2N_S} n_1 \left( (2N_SN_U + N_SN_UM_S)^2 + 2N_U + N_S + (3N_U + 1)(2N_SN_U + N_SN_UM_S) \right) \ln(1/\varepsilon_1) \right). \tag{58}$$

$$\tau_2 = O\left(\sqrt{7N_U + 2M_R + 2} n_2 \left( (M_R^2 + 2N_S)^2 + (3N_U + M_R + 1)(M_R^2 + 2N_S) + 2N_U + (M_R + 1)^2 \right) \ln(1/\varepsilon_2) \right). \tag{59}$$

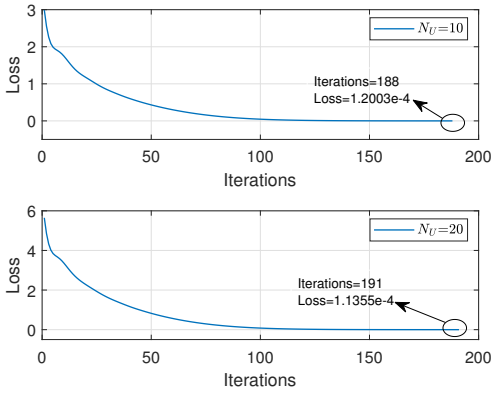


Fig. 3. Convergence rate of deep learning phase in TJPO.

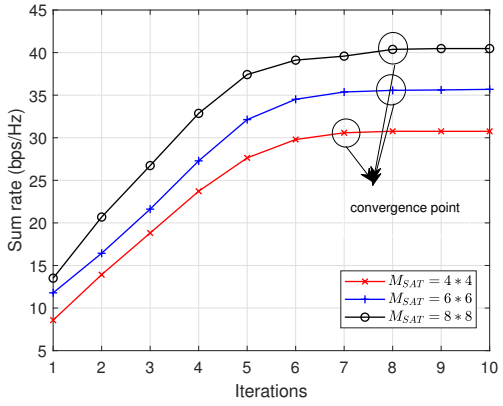


Fig. 4. Convergence rate of AO phase in TJPO.

- RIS with maximum ratio combination (MRC) (MRC-RIS): User association and RIS phase are performed by *Algorithm 2* and *Algorithm 4*, respectively. The beamforming vector is obtained using MRC method [38], where the beamforming vector of each user is

$$\mathbf{w}_{m,k} = \sqrt{\frac{P_0}{\sum_{k=1}^{N_U} a_{m,k}}} \frac{\mathbf{h}_{m,k}^H}{|\mathbf{h}_{m,k}|}. \tag{60}$$

- RIS with maximum remaining time (MRT-RIS): In this baseline, each terrestrial user is associated with the LEO satellite with maximum remaining time of connectivity. Meanwhile, beamforming and RIS phase shift are optimized by *Algorithm 3* and *Algorithm 4*, respectively.

Simulations are executed 100 times repeatedly with random starts, potentially leading to an average result that closely estimates the true mean.

### A. Convergence Performance Analyses

First, the convergence of the proposed algorithms for solving the subproblems of user association, beamforming and RIS phase design are verified. For each simulation, we generate the training dataset for DNN using 1000 data samples including user positions, satellite positions and user association schemes. Fig. 3 displays the convergence pattern of *Algorithm 2* using the training dataset with 10 and 20 terrestrial users, respectively. With the progression of iterations, it becomes evident, as shown in Fig. 3, that *Algorithm 2* typically reaches convergence around 200 iterations. Specifically, *Algorithm 2* converges at the 188-th iteration to $1.2003 \times 10^{-4}$ when $N_U = 10$ and the 191-st iteration to $1.1355 \times 10^{-4}$ when $N_U = 20$. Results show that the increase in terrestrial users escalates both the loss and computation complexity.

Fig. 4 elaborates the convergence behavior of the AO phase in *Algorithm 1* for three scenarios of $M_S = \{4\times4, 6\times6, 8\times8\}$. *Algorithm 1* converges within finite iterations for simulated parameter values. We also observe that the convergence speed of *Algorithm 1* is non-decreasing with the increasing of the number of satellite antennas, since increase in the number of LEO satellite antennas results in an increase in the dimensionality of the channel matrix, leading to a subsequent rise in computational complexity. The observed phenomenon provides empirical evidence supporting the accuracy of our computational complexity analysis. Meanwhile, Fig. 4 also shows that, a larger $M_S$ leads to a higher sum rate due to increased antenna gain amplitudes and higher degrees of freedom, which effectively reduce interference between terrestrial users. The results demonstrate that our proposed algorithms exhibit low complexity and achieve fast convergence, which are suitable for highly dynamic ULSNs.

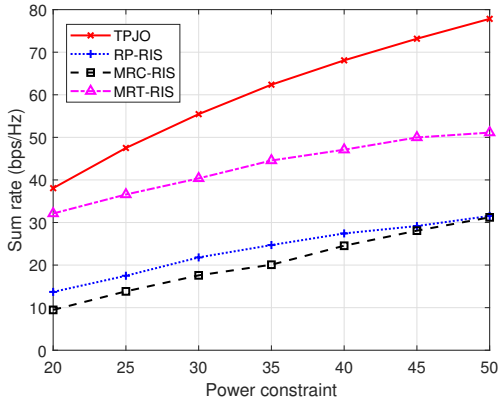


Fig. 5. Sum rate versus the transmit power constraint of LEO satellites.

### B. Sum Rate Analyses

Fig. 5 presents a comparison of the sum rate versus maximum transmission power of LEO satellite, where $P_0 = \{30, 35, 40, 45, 50\}$dBm with fixed $N_U = 30$ under different algorithms. The sum rate of ULSN increases with the transmission power of LEOs and the increase rate decreases with the increase in power. When the power is small, noise occupies the main part in SINR, the SINR increases dramatically with the value of the signal power received by the user, leading to the sharp increase in sum rate. When the limiting power of the LEO satellite is large, the interference power will increase accordingly when the received channel power increases, and at this time the enhancement of the sum rate by increasing the power is limited. The MRC-RIS algorithm adopts an equal

This article has been accepted for publication in IEEE Internet of Things Journal. This is the author's version which has not been fully edited and content may change prior to final publication. Citation information: DOI 10.1109/JIOT.2025.3532342



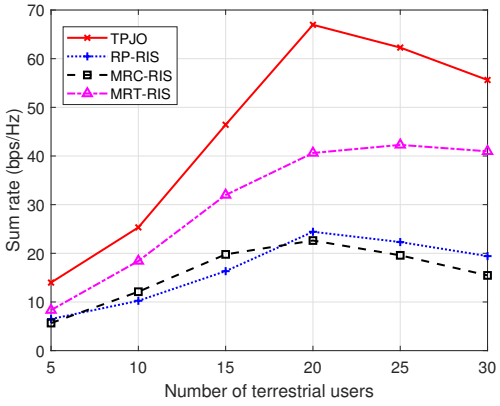


Fig. 6. Sum rate versus the number of terrestrial users in ULSN.

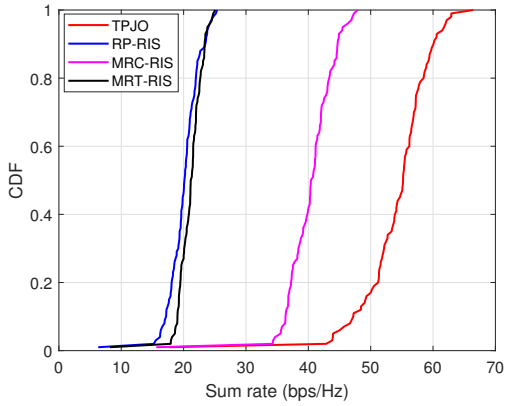


Fig. 7. CDF of the sum rate in ULSN.

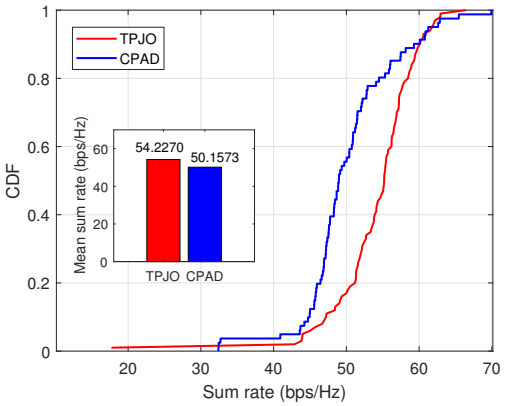


Fig. 8. Sum rate CDF of TPJO and CPAD algorithms.

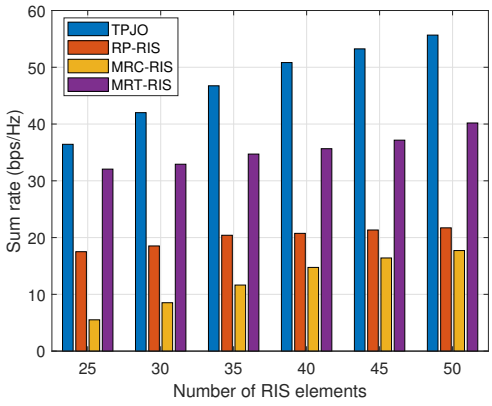


Fig. 9. Sum rate verse the number of RIS elements.

power distribution strategy, which limits the ability to reduce interference by simply increasing the total transmission power.

We compare the sum rate of the proposed TPJO with other baselines with the number of terrestrial users as $N_U = \{5, 10, 15, 20, 25, 30\}$, where other parameters are set fixed as aforementioned. Fig. 6 shows that the sum rate of the ULSN increases and then decreases slowly as the number of users increases for all scenarios. The sum rate of ULSN reaches its maximum value when the number of users is 20. When the number of users is small, the sum rate of ULSN increases due to the increase in the number of terrestrial users. But as the number of terrestrial users increases, for each user, the number of terrestrial users interfering with it increases and this aggregate the interference in SINR. And due to the transmission power limitations of LEO satellites, the transmission power allocated to transmit data to each user decreases accordingly. And the sum rate of ULSN decreases when the number of terrestrial users is more than 20.

Fig. 7 shows the cumulative distribution function (CDF) of the sum rate of algorithms including TPJO, RP-RIS, MRC-RIS and MRT-RIS regarding 30 terrestrial users. It can be observed that the sum rate proposed TPJO algorithm is superior to other baselines. Although MRC effectively eliminates inter-satellite interference, it cannot fully eliminate the influence of intra-satellite interference. This limitation hampers the overall sum rate performance. Meanwhile, MRT-RIS may lead to uneven user association of LEO satellites, the ability to mitigate interference between terrestrial users is limited due to the limited transmission power of LEO satellites compared with TJPO. Overall, the TPJO algorithm outperforms the other baselines, suggesting that its approach to optimizing user association, beamforming, and RIS phase shift is more effective for enhancing network throughput in the given scenarios.

Moreover, we compare our proposed TPJO with continuous relaxation-based alternating decent (CPAD) algorithm [39] for solving the MIP algorithm. In CPAD, each binary integer variable is relaxed to continuous variables in the range $[0, 1]$, and a penalty term is introduced in the objective function to approximate the original integer constraints. Then we compare the simulation results of TPJO with CPAD algorithm in terms of sum rate CDF. As shown in Fig. 8, the CDF curve for TPJO is mostly positioned to the right of the CDF curve for CPAD, indicating that TPJO achieves a higher sum rate at the same cumulative probability level. In the inset bar chart, the mean sum rates for TPJO and CPAD are displayed, with TPJO achieving an average sum rate higher than that of CPAD. Overall, TPJO outperforms CPAD both in sum rate distribution and mean performance, suggesting that TPJO enables greater spectral efficiency and transmission rates. This improvement is due to the fact that the relaxation of integer variables in CPAD

This article has been accepted for publication in IEEE Internet of Things Journal. This is the author's version which has not been fully edited and content may change prior to final publication. Citation information: DOI 10.1109/JIOT.2025.3532342



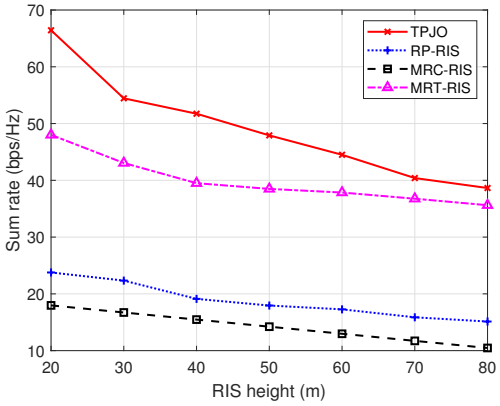


Fig. 10. Sum rate verse the deployment height of RIS elements.

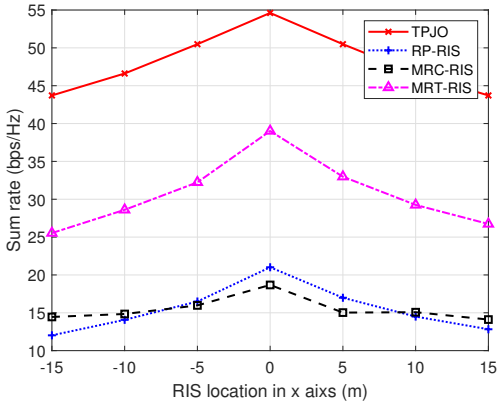


Fig. 11. Sum rate verse the deployment location of RIS elements.

may lead to discrepancies in the objective function, impacting the performance of the optimized sum rate.

### C. RIS Deployment

Fig. 9 presents the sum rate of the ULSN versus the number of RIS elements when $N_U = 30$ and $P_0 = 30$ dBm. It can be seen that the sum rate increases with the number of RIS elements $M_R$ increasing from 25 to 50. As observed, TPJO consistently outperforms the other algorithms across all RIS element counts, indicating its superior capability in leveraging RIS for enhanced sum rate. The sum rate of the ULSN achieved by the RP-RIS algorithm fluctuates while others increase with the increase in the number of RIS elements. This is because that the increase in the number of RIS elements may introduce interference in RP-RIS and reduce the sum rate. And the MRC-RIS displays the lowest sum rate which means MRC-RIS might not fully exploit the potential of RIS to mitigate interference between terrestrial users.

Meanwhile, Fig. 10 shows the relationship between sum rate and the deployment height of RIS elements when $N_U = 30$ and $P_0 = 30$ dBm. Without loss of generality, the elements of the RIS are located on the x-z plane and the coordination of RIS is set as $(0, 0, r_e + z_R)$ where $z_R$ is the height of RIS ranging from $z_R = 20m$ to $z_R = 80m$. Results reveals that as the deployment height of the RIS decreases, there is a greater gain in the overall sum rate. This phenomenon can be attributed to the impact of LSF. The closer proximity of the RIS to terrestrial users enhances the signal quality, mitigating the detrimental effects of LSF and resulting in increased overall sum rates. However, it is important to note that when RIS is deployed at low height, it can also be affected by NLOS conditions. Therefore, it is crucial to determine the appropriate height for RIS deployment, which strikes a balance between avoiding significant LSF and minimizing the probability of NLOS between the RIS and LEO satellites.

Fig. 11 shows the relationship between sum rate and the deployment location of the RIS in $x$-axis when $N_U = 30$ and $P_0 = 30$ dBm. RIS is deployed closer to the center of the multiple terrestrial users in ULSN, the sum rate of the system increases. This indicates that the system performance can be significantly enhanced by strategically selecting the location of the RIS with respect to the terrestrial user distribution. By carefully choosing the RIS deployment location, the signal quality and coverage can be optimized, leading to improved overall system performance and increased sum rates.

## VI. Conclusion

With the development of ULSNs for urban environments, RIS, as a new technology, will play an increasingly important role in future satellite communications. In this work, we have investigated the downlink MIMO data transmissions in ULSNs aided by RIS. To maximize the sum rate of terrestrial users, we have proposed an MIP model taking into account both the power constraint of LEOs and the rate constraint of terrestrial users. We have designed the TPJO algorithm to solve the MIP problem where DNN is used to optimize the user association matrix in deep learning phase, while SCA is used for joint beamforming optimization and RIS reflecting design in the AO phase. Simulation results demonstrate that the proposed TPJO algorithm achieves higher sum rate in comparison with baselines. In the future, we will consider robust beamforming and RIS reflecting design in the case of imperfect CSI, and the handover issues with time-variant system regarding high mobility of LEO satellites.

## References

[1] X. Qin, T. Ma, Z. Tang, X. Zhang, H. Zhou, and L. Zhao, "Service-aware resource orchestration in ultra-dense LEO satellite-terrestrial integrated 6G: A service function chain approach," *IEEE Transactions on Wireless Communications*, vol. 22, no. 9, pp. 6003–6017, 2023.

[2] R. Wang, M. A. Kishk, and M.-S. Alouini, "Ultra-dense LEO satellite-based communication systems: A novel modeling technique," *IEEE Communications Magazine*, vol. 60, no. 4, pp. 25–31, 2022.

[3] X. Zhang, B. Qian, X. Qin, T. Ma, J. Chen, H. Zhou, and X. S. Shen, "Cybertwin-assisted mode selection in ultra-dense LEO integrated satellite-terrestrial network," *Journal of Communications and Information Networks*, vol. 7, no. 4, pp. 360–374, 2022.

[4] T. Ma, B. Qian, X. Qin, X. Liu, H. Zhou, and L. Zhao, "Satellite-terrestrial integrated 6G: An ultra-dense LEO networking management architecture," *IEEE Wireless Communications*, pp. 1–8, 2022.

[5] Y. Seyedi, M. Shirazi, A. Moharrer, S. M. Safavi, and H. Amindavar, "Use of shadowing moments to statistically model mobile satellite channels in urban environments," *IEEE Transactions on Wireless Communications*, vol. 12, no. 8, pp. 3760–3769, 2013.

[6] 3GPP, "Study on New Radio (NR) to support non-terrestrial netwok," 3rd Generation Partnership Project (3GPP), Technical report (TR) 38.811, 9 2020, version 15.4.0.

[7] P. Ramezani, B. Lyu, and A. Jamalipour, "Toward RIS-enhanced integrated terrestrial/non-terrestrial connectivity in 6G," *IEEE Network*, pp. 1–9, 2022.

[8] J. Wang, Y.-C. Liang, Y. Pei, and X. Shen, "Reconfigurable intelligent surface as a micro base station: A novel paradigm for small cell networks," *IEEE Transactions on Wireless Communications*, vol. 22, no. 4, pp. 2338–2351, 2023.

[9] J. Ye, J. Qiao, A. Kammoun, and M.-S. Alouini, "Nonterrestrial communications assisted by reconfigurable intelligent surfaces," *Proceedings of the IEEE*, vol. 110, no. 9, pp. 1423–1465, 2022.

[10] K. W. Cho, Y. Ghasempour, and K. Jamieson, "Towards dual-band reconfigurable metasurfaces for satellite networking," in *Proceedings of the 21st ACM Workshop on Hot Topics in Networks*, 2022, pp. 17–23.

[11] E. Björnson, z. Özdogan, and E. G. Larsson, "Intelligent reflecting surface versus decode-and-forward: How large surfaces are needed to beat relaying?" *IEEE Wireless Communications Letters*, vol. 9, no. 2, pp. 244–248, 2020.

[12] X. Zhang, T. Ma, X. Qin, Y. Wang, and H. Zhou, "Reflecting intelligent surface aided downlink transmission in ultra-dense LEO satellite networks," in *2023 IEEE 23rd International Conference on Communication Technology (ICCT)*, 2023, pp. 1123–1128.

[13] K. Tekbiyik, G. K. Kurt, A. R. Ektı, and H. Yanikomeroglu, "Reconfigurable intelligent surfaces empowered THz communication in LEO satellite networks," *IEEE Access*, vol. 10, pp. 121 957–121 969, 2022.

[14] K. Tekbıyık, G. K. Kurt, A. R. Ekti, and H. Yanikomeroglu, "Reconfigurable intelligent surfaces in action for nonterrestrial networks," *IEEE Vehicular Technology Magazine*, vol. 17, no. 3, pp. 45–53, 2022.

[15] B. Zheng, S. Lin, and R. Zhang, "Intelligent reflecting surface-aided LEO satellite communication: Cooperative passive beamforming and distributed channel estimation," *IEEE Journal on Selected Areas in Communications*, vol. 40, no. 10, pp. 3057–3070, 2022.

[16] K. Tekbıyık, G. K. Kurt, and H. Yanikomeroglu, "Energy-efficient RIS-assisted satellites for IoT networks," *IEEE Internet of Things Journal*, vol. 9, no. 16, pp. 14 891–14 899, 2022.

[17] H. Dong, C. Hua, L. Liu, W. Xu, and R. Tafazolli, "Intelligent reflecting surface-aided integrated terrestrial-satellite networks," *IEEE Transactions on Wireless Communications*, vol. 22, no. 4, pp. 2507–2522, 2023.

[18] S. Xu, J. Liu, Y. Cao, J. Li, and Y. Zhang, "Intelligent reflecting surface enabled secure cooperative transmission for satellite-terrestrial integrated networks," *IEEE Transactions on Vehicular Technology*, vol. 70, no. 2, pp. 2007–2011, 2021.

[19] R. Deng, B. Di, H. Zhang, H. V. Poor, and L. Song, "Holographic MIMO for LEO satellite communications aided by reconfigurable holographic surfaces," *IEEE Journal on Selected Areas in Communications*, vol. 40, no. 10, pp. 3071–3085, 2022.

[20] X. Liu, B. Zhao, M. Lin, J. Ouyang, J.-B. Wang, and J. Wang, "IRS-aided uplink transmission scheme in integrated satellite-terrestrial networks," *IEEE Transactions on Vehicular Technology*, vol. 72, no. 2, pp. 1847–1861, 2023.

[21] Z. Lin, H. Niu, K. An, Y. Wang, G. Zheng, S. Chatzinotas, and Y. Hu, "Refracting RIS-aided hybrid satellite-terrestrial relay networks: Joint beamforming design and optimization," *IEEE Transactions on Aerospace and Electronic Systems*, vol. 58, no. 4, pp. 3717–3724, 2022.

[22] L. You, K.-X. Li, J. Wang, X. Gao, X.-G. Xia, and B. Ottersten, "Massive MIMO transmission for LEO satellite communications," *IEEE Journal on Selected Areas in Communications*, vol. 38, no. 8, pp. 1851–1865, 2020.

[23] K. An, M. Lin, T. Liang, J.-B. Wang, J. Wang, Y. Huang, and A. L. Swindlehurst, "Performance analysis of multi-antenna hybrid satellite-terrestrial relay networks in the presence of interference," *IEEE Transactions on Communications*, vol. 63, no. 11, pp. 4390–4404, 2015.

[24] X. Sui, Z. Jiang, Y. Lyu, R. Fan, H. Hu, and Z. Liu, "Integrating convex optimization and deep learning for downlink resource allocation in LEO satellites networks," *IEEE Transactions on Cognitive Communications and Networking*, pp. 1–1, 2024.

[25] H. Yang, S. Liu, L. Xiao, Y. Zhang, Z. Xiong, and W. Zhuang, "Learning-based reliable and secure transmission for UAV-RIS-assisted communication systems," *IEEE Transactions on Wireless Communications*, pp. 1–1, 2023.

[26] Q. Bie, Z. Liang, Y. Liu, Q. Wu, X. Zhao, and X. Y. Zhang, "User association for reconfigurable intelligent surfaces aided cell-free networks," *IEEE Transactions on Vehicular Technology*, pp. 1–13, 2023.

[27] S. Zhang, A. Liu, C. Han, X. Ding, and X. Liang, "A network-flows-based satellite handover strategy for LEO satellite networks," *IEEE Wireless Communications Letters*, vol. 10, no. 12, pp. 2669–2673, 2021.

[28] Z. Tang, K. Yu, G. Yang, L. X. Cai, and H. Zhou, "New bridge to cloud: An ultra-dense LEO assisted green computation offloading approach," *IEEE Transactions on Green Communications and Networking*, vol. 7, no. 2, pp. 552–564, 2023.

[29] L.-N. Tran, M. F. Hanif, A. Tolli, and M. Juntti, "Fast converging algorithm for weighted sum rate maximization in multicell MISO downlink," *IEEE Signal Processing Letters*, vol. 19, no. 12, pp. 872–875, 2012.

[30] Q. Wu and R. Zhang, "Intelligent reflecting surface enhanced wireless network via joint active and passive beamforming," *IEEE Transactions on Wireless Communications*, vol. 18, no. 11, pp. 5394–5409, 2019.

[31] H. Zhou, X. Kang, Y.-C. Liang, S. Sun, and X. Shen, "Cooperative beamforming for reconfigurable intelligent surface-assisted symbiotic radios," *IEEE Transactions on Vehicular Technology*, vol. 71, no. 11, pp. 11 677–11 692, 2022.

[32] K.-Y. Wang, A. M.-C. So, T.-H. Chang, W.-K. Ma, and C.-Y. Chi, "Outage constrained robust transmit optimization for multiuser MISO downlinks: Tractable approximations by conic optimization," *IEEE Transactions on Signal Processing*, vol. 62, no. 21, pp. 5690–5705, 2014.

[33] B. Di, H. Zhang, L. Song, Y. Li, and G. Y. Li, "Ultra-dense LEO: Integrating terrestrial-satellite networks into 5G and beyond for data offloading," *IEEE Transactions on Wireless Communications*, vol. 18, no. 1, pp. 47–62, 2019.

[34] *SpaceX Non-Geostationary Satellite System*, Washington, DC, USA, 2016.

[35] Z. Li, F. Xiao, S. Wang, T. Pei, and J. Li, "Achievable rate maximization for cognitive hybrid satellite-terrestrial networks with AF-relays," *IEEE Journal on Selected Areas in Communications*, vol. 36, no. 2, pp. 304–313, 2018.

[36] T. Ma, B. Qian, X. Qin, X. Zhang, L. X. Cai, and H. Zhou, "Resource scheduling for high-capacity multicast service in ultra-dense LEO satellite networks," *IEEE Transactions on Vehicular Technology*, pp. 1–14, 2023.

[37] Z. Wang, Y. Cao, D. Zhang, X. Hua, P. Gao, and T. Jiang, "User selection for MIMO downlink with digital and hybrid maximum ratio transmission," *IEEE Transactions on Vehicular Technology*, vol. 70, no. 10, pp. 11 101–11 105, 2021.

[38] H. H. M. Tam, H. D. Tuan, D. T. Ngo, T. Q. Duong, and H. V. Poor, "Joint load balancing and interference management for small-cell heterogeneous networks with limited backhaul capacity," *IEEE Transactions on Wireless Communications*, vol. 16, no. 2, pp. 872–884, 2017.


**Xin Zhang** (Student Member, IEEE) received the B.S. degree in basic science of mathematics and physics from University of Electronic Science and Technology of China, Chengdu, China, in 2020. She is currently working toward the Ph.D. degree in communications and information system with Nanjing University, Nanjing, China. Her research interests include space-air-ground integrated networks, resource allocation and convex optimization theory.

**Xiaohan Qin** (Student Member, IEEE) received the B.S. degree in communication engineering from Central South University, Changsha, China, in 2020. She is currently working toward the Ph.D. degree in communications and information system with Nanjing University, Nanjing, China. Her research interests include space-air-ground integrated networks, network resource management and game theory.

**Zitian Zhang** received his B.S. and Ph.D. degree in 2010 and 2016 from Shanghai Jiao Tong University. After his Ph.D. program. He is currently an associate professor at Zhejiang Gongshang University. He worked as a research engineer in China Aeronautical Radio Electronics Research Institute from 2016 to 2017. From 2018 to 2020, he was with East China University of Science and Technology. From 2020 to 2022, he was a Mary Curie research fellow at the Ranplan Wireless Network Design Ltd. His research interests include deep learning, big data analytics, and device-to-device communications.

**Lin X. Cai** (Senior Member, IEEE) received the M.A.Sc. and Ph.D. degrees in electrical and computer engineering from the University of Waterloo, Waterloo, ON, Canada, in 2005 and 2010, respectively. She is currently an Associate Professor with the Department of Electrical and Computer Engineering, Illinois Institute of Technology, Chicago, IL, USA. Her research interests include green communication and networking, intelligent radio resource management, and wireless Internet of Things.

Dr. Cai was the recipient of the Postdoctoral Fellowship Award from the Natural Sciences and Engineering Research Council of Canada in 2010, the Best Paper Award from the IEEE GLOBECOM 2011, the NSF Career Award in 2016, and the IIT Sigma Xi Research Award in the Junior Faculty Division in 2019. She is an Executive Editorial Committee Member of IEEE Transactions on Wireless Communications, an Associate Editor of IEEE Transactions on Vehicular Technology, and the co-chair of IEEE conferences.

**Haibo Zhou** (Senior Member, IEEE) received the Ph.D. degree in information and communication engineering from Shanghai Jiao Tong University, Shanghai, China, in 2014. From 2014 to 2017, he was a Postdoctoral Fellow with the Broadband Communications Research Group, Department of Electrical and Computer Engineering, University of Waterloo. He is currently a Full Professor with the School of Electronic Science and Engineering, Nanjing University, Nanjing, China. He was a recipient of the 2019 IEEE ComSoc Asia-Pacific Outstanding Young Researcher Award. He served as Track/Symposium Co-Chair for IEEE/CIC ICCC 2019, IEEE VTC-Fall 2020, IEEE VTC-Fall 2021, and IEEE GLOBECOM 2022. He is currently an Associate Editor of the IEEE Transactions on Wireless Communications, IEEE Internet of Things Journal, IEEE Network Magazine, and IEEE Wireless Communications Letter. His research interests include resource management and protocol design in B5G/6G networks, vehicular ad hoc networks, and space-air-ground integrated networks.

**Weihua Zhuang** (Fellow, IEEE)received the B.Sc. and M.Sc. degrees from Dalian Maritime University, China, and the Ph.D. degree from the University of New Brunswick, Canada, all in electrical engineering. Since 1993, she has been a faculty member in the Department of Electrical and Computer Engineering, University of Waterloo, Canada, where she is a University Professor and a University Research Chair in wireless communication networks. Her current research focuses on network architecture, algorithms and protocols, and service provisioning in future communication systems. She is the recipient of Women's Distinguished Career Award in 2021 from IEEE Vehicular Technology Society, R.A. Fessenden Award in 2021 from IEEE Canada, Award of Merit in 2021 from the Federation of Chinese Canadian Professionals (Ontario), and Technical Recognition Award in Ad Hoc and Sensor Networks in 2017 from IEEE Communications Society.

Dr. Zhuang is a Fellow of the IEEE, Royal Society of Canada (RSC), Canadian Academy of Engineering (CAE), and Engineering Institute of Canada (EIC). She is the President and an elected member of the Board of Governors (BoG) of the IEEE Vehicular Technology Society. She was the Editor-in-Chief of IEEE Transactions on Vehicular Technology (2007-2013), an editor of IEEE Transactions on Wireless Communications (2005-2009), General Co-Chair of IEEE/CIC International Conference on Communications in China (ICCC) 2021, Technical Program Committee (TPC) Chair/Co-Chair of IEEE Vehicular Technology Conference 2017 Fall and 2016 Fall, TPC Symposia Chair of the IEEE Globecom 2011, and an IEEE Communications Society Distinguished Lecturer (2008-2011).